Turk. J. Math. Comput. Sci.
17(1)(2025) 102–119
© MatDer
DOI : 10.47000/tjmcs.1617287

Investigation of a Water-based Boron Nanofluid Inside a Cavity with an Obstacle Using a Numerical Technique

Yücel Baltürk[1], İnci Çilingir Süngü[2,*], Hüseyin Demir[3]

[1]*Repuplic of Türkiye Ministry of National Education, Samsun Science and Art Center, 55070, Samsun, Türkiye.*
[2]*Department of Mathematics and Natural Sciences Education, Faculty of Education, Ondokuz Mayıs University, 55200, Samsun, Türkiye.*
[3]*Department of Software Engineering, Faculty of Engineering and Natural Sciences, Samsun University, 55420, Samsun, Türkiye.*

Received: 10-01-2025 • Accepted: 11-04-2025

Abstract. In this paper the stability of two-dimensional fluid flow induced by various wall movements was thoroughly investigated within a planar cavity for steady-state water-based boron nanofluids with respect to the aspect ratio. The nonlinear governing equations describing the flow were numerically evaluated using the Successive Over-Relaxation (SOR) method combined with the finite-difference approach. The relationship between velocity and pressure was represented through the stream function-vorticity formulation. Special emphasis was placed on optimising numerical procedures for two different aspect ratios to ensure solution accuracy. Simulations were conducted for a range of Reynolds numbers to predict the behaviour of streamlines in the flow domain. The results were compared with those from previous studies on Newtonian fluids, showing reliable agreement. Additionally, the behaviour of water-based boron nanofluids in wall-driven flow with an obstacle in a flow domain was documented for the first time, providing novel insights into the flow dynamics. These findings serve as a foundation for upcoming research on nanofluids in fluid dynamics. The results also contribute to advancing the understanding of nanofluid behaviour in wall-driven flow. Graphical data demonstrated the reliability and accuracy of the finite-difference method coupled with the SOR approach in solving complex fluid dynamics problems.

2020 AMS Classification: 35Q30, 76M20, 76A99

Keywords: Boron Nanofluids, Lid-Driven flow, FDM, SOR method.

1. Introduction

The production of nanofluids incorporating various nanoparticles plays a pivotal role in advancing modern technology, providing substantial benefits by improving the efficiency and control of fluid motion in various systems. Due to their adaptable and versatile properties, nanofluids have garnered significant attention in scientific research. This growing interest is reflected in the continuous increase of studies focused on optimizing nanofluid performance across multiple applications, including energy transfer, cooling systems and biomedical technologies. In parallel with the growing interest in nanofluid applications, the behaviour of these fluids in confined systems, such as closed cavities, continues to be a critical area of study. The system, governed by elliptical partial differential equations, is typically solved using various numerical methods to predict the flow dynamics. For instance, Batchelor (1956) [2] examined

*Corresponding Author
Email addresses: yucelbalturk@gmail.com (Y. Baltürk), incicilingir@gmail.com (İ. Çilingir Süngü), huseyin.demir@samsun.edu.tr (H. Demir)

steady-state and laminar flow over a wide range of Reynolds numbers, even extending toward infinity. Kawaguti [10] introduced the first numerical approximation for the Navier-Stokes equations, while Peaceman and Rachford [15] applied the alternating direction implicit method to solve parabolic and elliptic equations. Lid-driven flow problems are particularly valuable as benchmarks in testing and validating these numerical methods. Burggraf's 1966 study [4] on steady separated flows provides important insights into the structure of these flows. A substantial body of studies investigated the effects of wall motion on fluid dynamics, with numerous significant contributions documented in the literature [6–9]. The effects of cavity shape variations on instability were thoroughly examined through studies that focused on changes in the aspect ratio. One of the most seminal studies in this area was conducted by Pan in 1967 [14], which considerably advanced the understanding of this phenomenon. Additionally, the influence of obstacles within the cavity was carefully explored in several subsequent studies. With advancing technology, studies investigating nanofluids, which enabled the production of fluids tailored to specific needs, gained significant prominence in the literature. Both experimental and theoretical studies commonly used Al2O3, CuO, Al, and Cu nanoparticles to create nanofluids. Fluid research was primarily conducted through experimental methods. Such as the studies by Li [11] and Cacua [5], which were among the noteworthy contributions in this field. The numerical solution techniques employed to determine the heat transfer properties in square cavities were well-documented in the literature, particularly in the works of Öztop [13] and Abad [1]. Meanly the behaviour of nanofluids were examined by comparing them with the behaviour of Newtonian fluids both in experimental and theoretical works. In the literature, the Navier-Stokes equations were considered in theoretical works. In the real world, the lid-driven problem is modelled in many industrial processes such as short dwell and flexible blade coaters and in materials processing, dynamics of lakes, metal casting, galvanizing and some airport runways [18]. Lid-driven flow in a square cavity is also used as a preliminary study to investigate two-dimensional incompressible fluid behaviour. In particular, it is used to understand the behaviour of more complex fluids such as roll coating, shrinkage flows and flow behaviour defined over a slit [2]. To resolve the specialized system of equations the Lattice Boltzmann Method, Finite Volume Method and Finite Difference Method were commonly used in literature. The studies on boron, which formed the basis of this paper, were carried out in recent years across various fields of industry and science. Some of these fields included chemistry, heat transfer, agriculture, alchemy and health.

This study aims to numerically solve wall motion problems for water-based Boron nanofluids within a cavity, considering two distinct aspect ratios of 1 and 0.33. A stationary obstacle fixed at the middle of the cavity was also included in the comprehensive analysis. The flow was assumed to be steady, incompressible and laminar. The governing motion equations were discretized with the central finite difference method and the generating system of linear equations was calculated with the successive over-relaxation (SOR) method. This approach allowed for an in-depth investigation of the lid-driven flow dynamics under the influence of moving walls for Boron/water nanofluid, with comparisons made to Newtonian fluids. Additionally, the study explored the variations in fluid motion within the cavity for aspect ratios of 1 and 0.33, considering Reynolds numbers of 1, 100, 1000 and 2000. The outcomes of this research significantly contribute to the understanding of nanofluid dynamics, particularly in confined geometries. These findings provide a foundation for optimizing nanofluid-based systems and highlight the importance of further investigations to improve the efficiency and functionality of such systems across various engineering applications.

2. Mathematical Model

2D incompressible flow equations for nanofluids were given as below

$$\nabla \cdot \vec{U} = 0,$$
$$\rho_{nf}\left(\vec{U}\cdot\nabla u\right) = -\frac{\partial P}{\partial x} + \mu_{nf}\nabla^2 u,$$
$$\rho_{nf}\left(\vec{U}\cdot\nabla v\right) = -\frac{\partial P}{\partial y} + \mu_{nf}\nabla^2 v,$$

where the pressure was noticed by P and $\vec{U} = (u, v)$ is the velocity vector. μ_{nf} is the viscosity of nanofluid. The density of the nanofluid is described as

$$\rho_{nf} = (1-\varphi)\rho_f + \varphi\rho_s.$$

The base fluid's density was shown with ρ_f and the solid particles' density was shown with ρ_s. he volume fraction of nanoparticles was noticed with φ. In this paper the Brinkman [3] viscosity model was preferred to compute the effective viscosity. The nanofluid's dynamic viscosity based on this model was calculated by using the formula

$$\mu_{eff} = \frac{\mu_f}{(1-\varphi)^{2.5}}.$$

Using dimensionless variables

$$\hat{x} = \frac{x}{H}, \ \hat{y} = \frac{y}{H}, \ \hat{u} = \frac{u}{U_0}, \ \hat{v} = \frac{v}{U_0}, \ \mathbf{\Omega} = \frac{\omega H^2}{\alpha_f}, \hat{p} = \frac{P}{\rho_{nf} {U_0}^2}, \Psi = \alpha_f \psi, \ \mathrm{Re} = \frac{\rho H U_0}{\mu}$$

the dimensionless form of equations of motion were obtained as

$$\hat{u}\frac{\partial \mathbf{\Omega}}{\partial \hat{x}} + \hat{v}\frac{\partial \mathbf{\Omega}}{\partial \hat{y}} = K_1 \frac{1}{\mathrm{Re}}\left(\frac{\partial^2 \mathbf{\Omega}}{\partial \hat{x}^2} + \frac{\partial^2 \mathbf{\Omega}}{\partial \hat{y}^2}\right),$$

$$-\mathbf{\Omega} = \frac{\partial^2 \Psi}{\partial \hat{x}^2} + \frac{\partial^2 \Psi}{\partial \hat{y}^2},$$

$$\hat{u} = \frac{\partial \Psi}{\partial \hat{y}}, \ \hat{v} = -\frac{\partial \Psi}{\partial \hat{x}},$$

where $K_1 = \frac{\mu_{nf}}{\nu_f \rho_{nf}} = \frac{\nu_{nf}}{\nu_f}$. In terms of plain notation, hat notation was not used in the rest of the study.

In this study the results were obtained for Newtonian fluids and the water-based Boron nanofluid with $\varphi = 0.15$ solid particle volume fraction. The values of density for water and boron were taken respectively as $\rho = 997.1 \left(kg/m^3\right)$ and $\rho = 2340 \left(kg/m^3\right)$ [12, 16]. The view of the cavity for lid driven problems was shown in Figure 1.

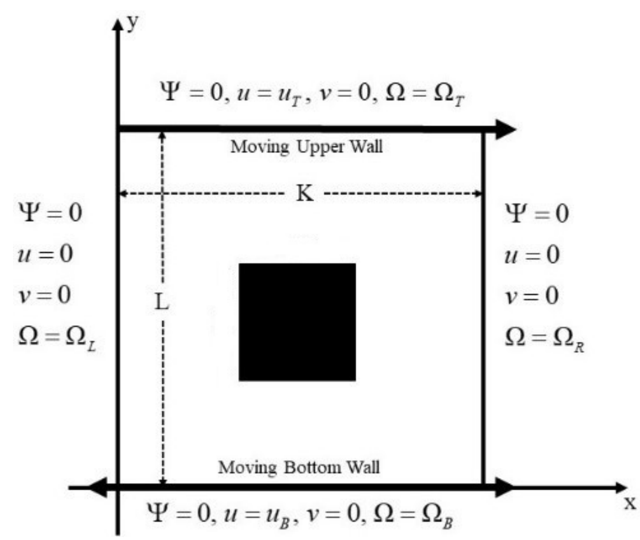

FIGURE 1. The representative image of moving walls in the cavities with a stationary obstacle.

The case featuring an obstacle at the centre of the cavity, with an aspect ratio of 1, was depicted in Figure 1. Additionally, when it preferred the aspect ratio is 0.33 the x axis was taken as 3 units long and the y axis was taken as 1 unit long. Velocity functions at the boundaries were defined as below

$$\begin{aligned} u = v &= 0 \quad \text{for} \quad x = 0, \quad 0 < y < L \\ u = v &= 0 \quad \text{for} \quad x = K, \quad 0 < y < L \\ u = u_B, \quad v &= 0 \quad \text{for} \quad y = 0, \quad 0 \le x \le K \\ u = u_T, \quad v &= 0 \quad \text{for} \quad y = L, \quad 0 \le x \le K. \end{aligned}$$

In this study, three distinct cases were meticulously investigated to examine the effects of wall motion on fluid dynamics, with a fixed obstacle positioned at the center of the cavity. The configurations are outlined as follows:

Case 1: This case addressed the motion of the upper wall alone, with velocity components set to $u_T = 1,\ u_B = 0$, establishing a controlled baseline structure for a preliminary exploration of flow dynamics.
Case 2: In this case, both the upper and bottom walls were actuated in opposite directions, with velocity components defined as $u_T = 1,\ u_B = -1$, facilitating the investigation of more intricate flow interactions.
Case 3: The final case involved the simultaneous motion of the upper and bottom walls in the same direction, with velocity components set to $u_T = u_B = 1$, enabling the analysis of flow behaviour under a uniform, synchronized motion.

The stream and vorticity functions on the boundary were given as

$$\Psi = 0,\ \frac{\partial \Psi}{\partial y} = 0,\ -\mathbf{\Omega} = \frac{\partial^2 \Psi}{\partial x^2} \text{ for } 0 < y < L \text{ on } x = 0 \text{ and } x = K$$

$$\Psi = 0,\ \frac{\partial \Psi}{\partial x} = 0,\ -\mathbf{\Omega} = \frac{\partial^2 \Psi}{\partial y^2} \text{ for } 0 \le x \le K \text{ on } y = 0 \text{ and } y = L.$$

In addition, $N = \frac{K}{Dx} + 1$ and $M = \frac{L}{Dy} + 1$, where Dx and Dy are the length of the grid spacing in the x axis and y axis direction, respectively. The discretization of the stream function using the FDM is given below.

$$\frac{\Psi(i+1,j) - 2\Psi(i,j) + \Psi(i-1,j)}{Dx^2} + \frac{\Psi(i,j+1) - 2\Psi(i,j) + \Psi(i,j-1)}{Dy^2} = -\mathbf{\Omega}(i,j), \tag{2.1}$$

$$u(i,j)\left(\frac{\mathbf{\Omega}(i+1,j) - \mathbf{\Omega}(i-1,j)}{2Dx}\right) + v(i,j)\left(\frac{\mathbf{\Omega}(i,j+1) - \mathbf{\Omega}(i,j-1)}{2Dy}\right) = \frac{K_1}{\mathrm{Re}}\left\{\begin{array}{l}\dfrac{\mathbf{\Omega}(i+1,j) - 2\mathbf{\Omega}(i,j) + \mathbf{\Omega}(i-1,j)}{Dx^2} \\ + \dfrac{\mathbf{\Omega}(i,j+1) - 2\mathbf{\Omega}(i,j) + \mathbf{\Omega}(i,j-1)}{Dy^2}\end{array}\right\}. \tag{2.2}$$

The discretization of boundary conditions for this problem was made as follows.

$$u(1,j) = v(1,j) = 0,\ j = 1..M+1, \tag{2.3}$$

$$u(N+1,j) = v(N+1,j) = 0,\ j = 1..M+1, \tag{2.4}$$

$$u(i,1) = u_B,\ v(i,1) = 0,\ i = 1..N+1, \tag{2.5}$$

$$u(i,M+1) = u_T, v(i,M+1) = 0,\ i = 1..N+1, \tag{2.6}$$

$$\Psi(1,j) = 0,\ \Psi(N+1,j) = 0,\ j = 1..M+1, \tag{2.7}$$

$$\Psi(i,1) = 0,\ \Psi(i,M+1) = 0,\ i = 1..N+1. \tag{2.8}$$

The vorticity function on the boundary was written in terms of the stream function as following:

$$\mathbf{\Omega}(1,j) = \frac{6Dxu(1,j) + \Psi(3,j) - 8\Psi(2,j)}{2Dx^2},\ j = 1..M+1, \tag{2.9}$$

$$\mathbf{\Omega}(N+1,j) = \frac{\Psi(N-1,j) - 8\Psi(N,j) - 6Dyu(N+1,j)}{2Dx^2},\ j = 1..M+1, \tag{2.10}$$

$$\mathbf{\Omega}(i,1) = \frac{\Psi(i,3) - 8\Psi(i,2)}{2Dy^2},\ i = 1..N+1, \tag{2.11}$$

$$\mathbf{\Omega}(i,M+1) = \frac{\Psi(i,M-1) - 8\Psi(i,M)}{2Dy^2},\ i = 1..N+1. \tag{2.12}$$

The discretized equations (2.1) and (2.2) with the boundary conditions (2.3)-(2.12), were solved numerically with SOR method by transforming them to a linear equation system. Here, the square and 0.33 aspect ratio cavities were introduced taking K = L and K = 3L, respectively. Moreover, the boundary conditions on the obstacle in the cavity were given as

$$\Psi(i, j) = 0, \ u(i, j) = 0, \ v(i, j) = 0.$$

Furthermore, the boundary conditions of vorticity function on the walls of obstacle were obtained via the stream function inside the cavity.

3. Results And Discussion

In this section, the numerical results of cavity-driven flow with various directions of motion for the upper and bottom walls were investigated for both Newtonian fluids and water-based Boron nanofluids in square and aspect ratio 0.33 cavities. For simplicity, these cases were referred to as Case 1, Case 2 and Case 3. The simulations were performed for Reynolds numbers of 1, 100, 1000 and 2000. Stream function contours for both Newtonian fluids and nanofluids were compared for aspect ratios of 1 and 0.33. Furthermore, graphical comparisons of the centerline velocity profiles were made for Reynolds numbers of 100 and 1000. The velocity profiles for the lid-driven cavity flow with Newtonian fluids, as obtained in this study, were presented in Figure 2, while the results from Tosoka and Kakuda (1994) [17] were shown in Figure 3. A close agreement was observed both qualitatively and quantitatively, confirming that the results from this study were fully consistent with the data reported by Tosoka and Kakuda.

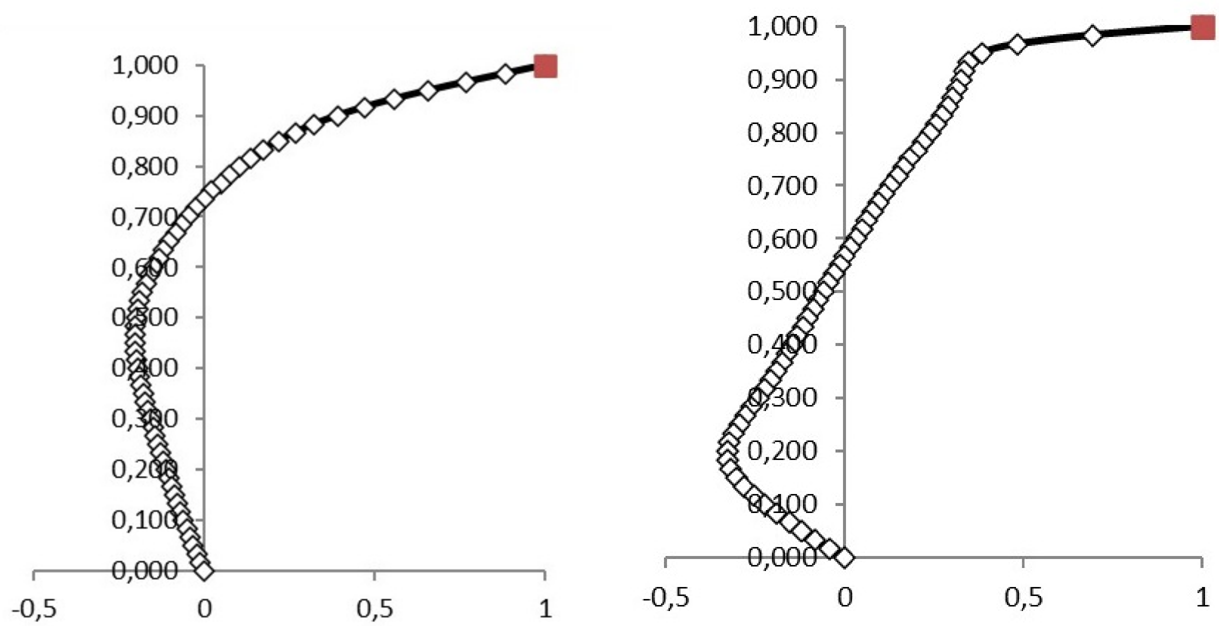

(i) Re=100 (ii) Re=1000

Figure 2. The velocity profile along vertical centreline at Re=100 and Re=1000 for Newtonian fluid by author

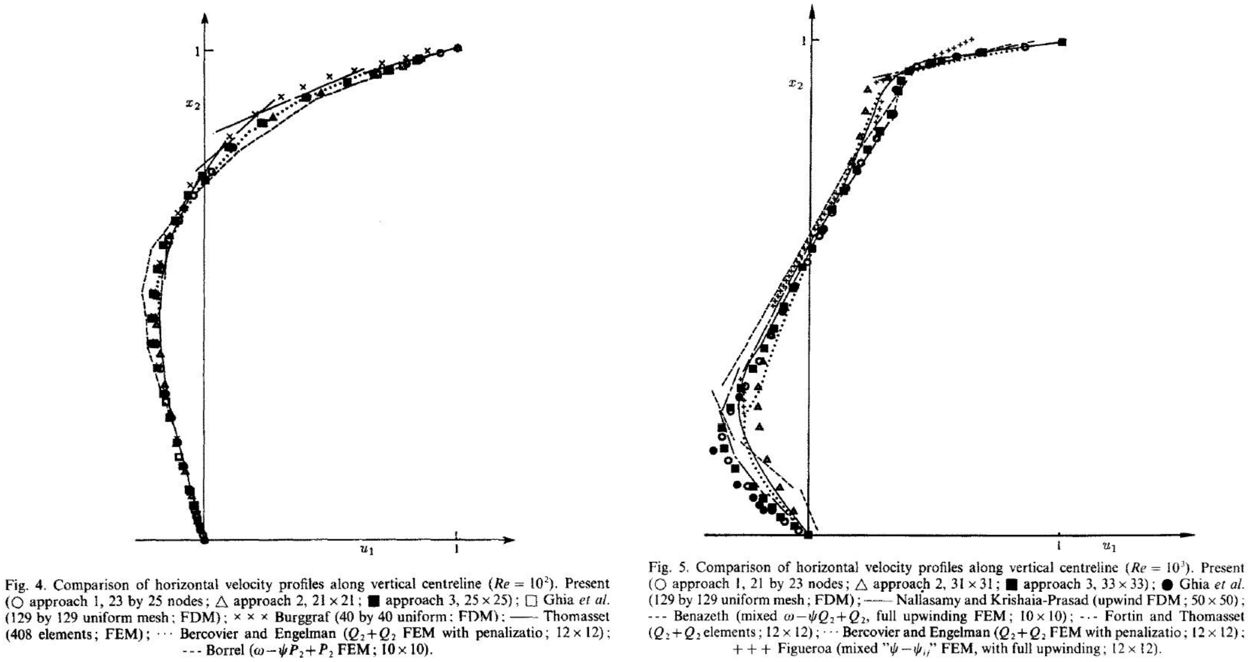

(i) Re=100 (ii) Re=1000

FIGURE 3. The velocity profile along vertical centreline at Re=100 and Re=1000 for Newtonian fluid by Tosoka and Kakuda, 1994 [17]

3.1. **Comparison of Streamlines When Aspect Ratio is 1.**

3.1.1. ***Case 1:*** *Movement of Upper Wall.*

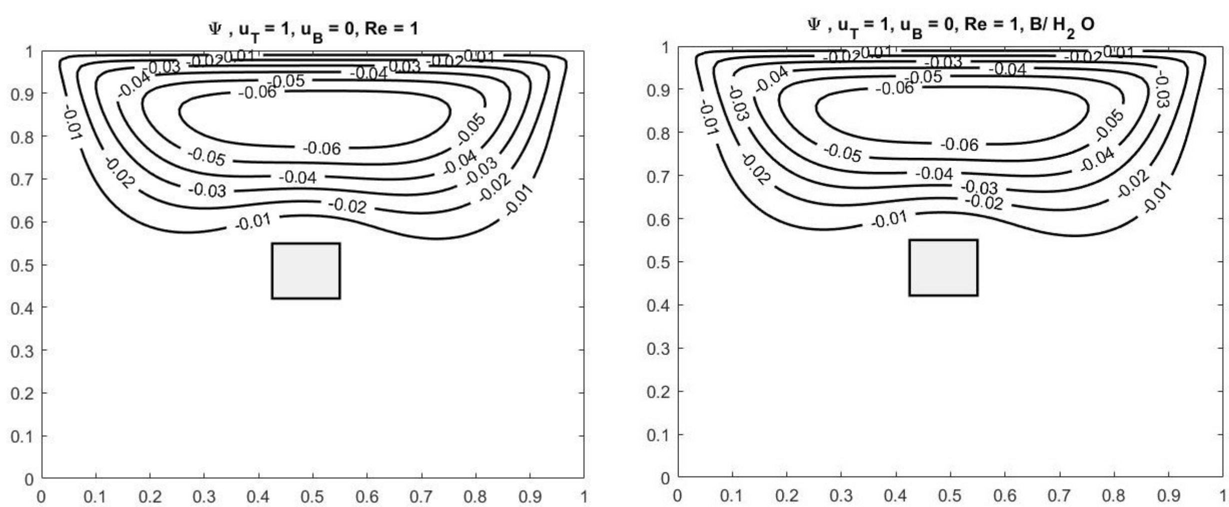

(i) (ii)

FIGURE 4. The streamlines for Newtonian Fluid (i) and Boron/Water Nanofluid (ii) at Re=1

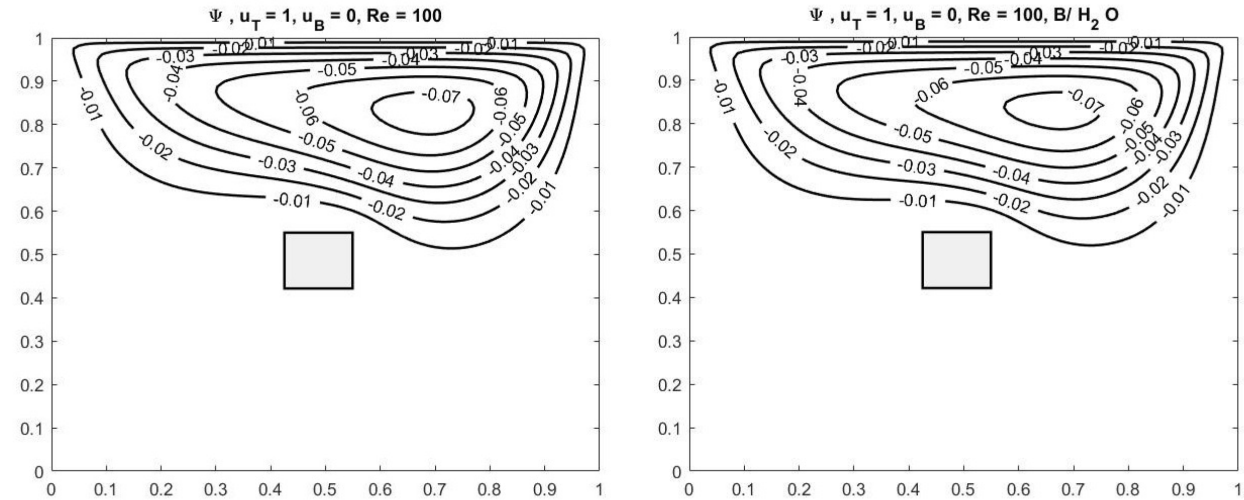

(i) (ii)

Figure 5. The streamlines for Newtonian Fluid (i) and Boron/Water Nanofluid (ii) at Re=100

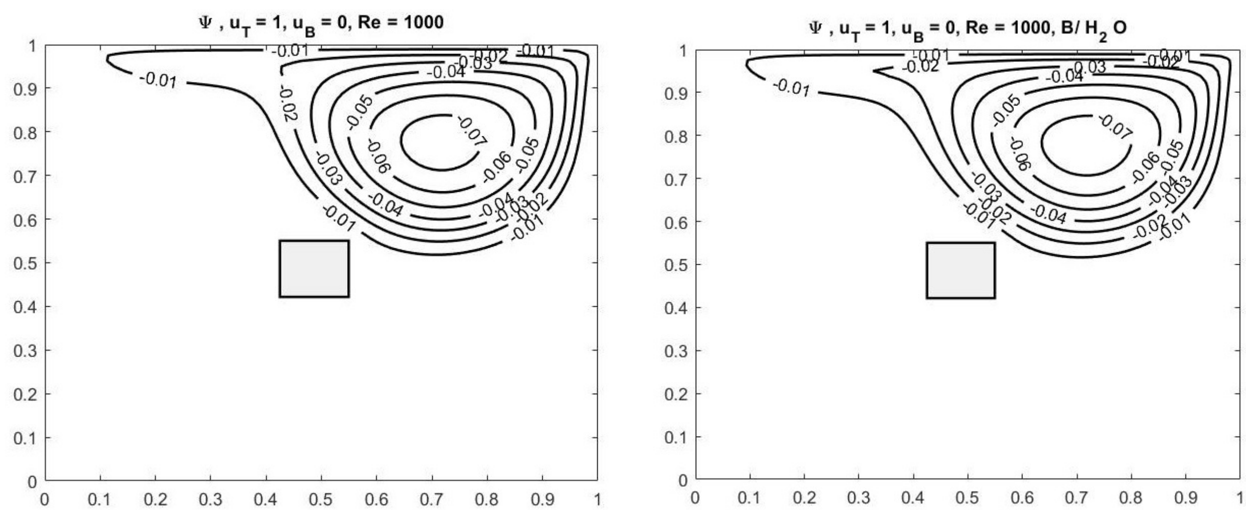

(i) (ii)

Figure 6. The streamlines for Newtonian Fluid (i) and Boron/Water Nanofluid (ii) at Re=1000

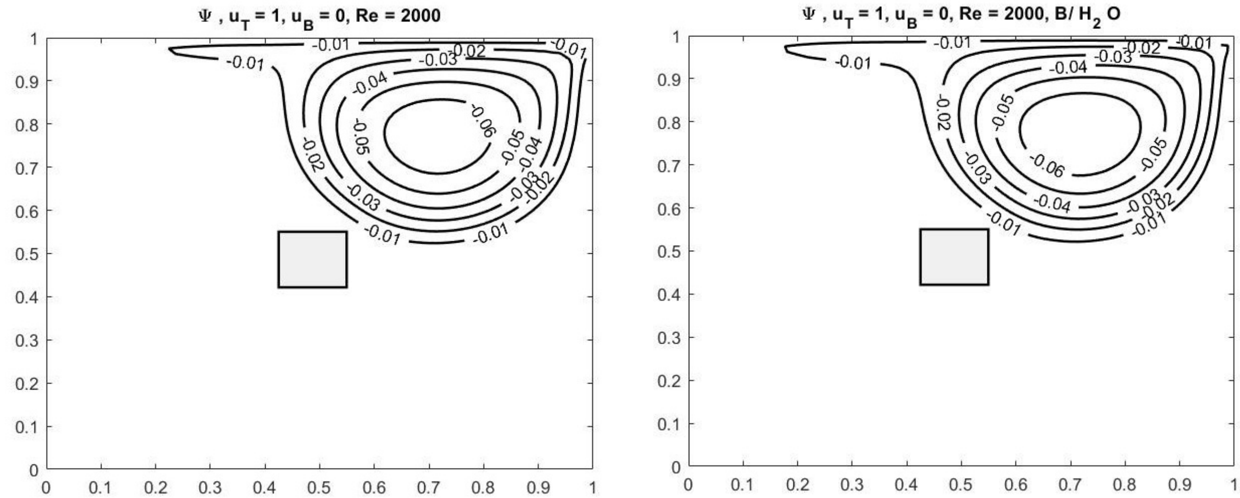

(I) (II)

Figure 7. The streamlines for Newtonian Fluid (I) and Boron/Water Nanofluid (II) at Re=2000

In Figures 4, 5, 6 and 7 the graphical representations of stream function contours for Newtonian fluid (I) and water-based Boron nanofluid (II) were shown at the values of Reynolds number 1, 100, 1000 and 2000 respectively. The results show that nanofluids affect streamlines like Newtonian fluids. At Re=1 the primary vortex settled at the center. At Re=100 it shifted to the upper right corner. The movement aligned with the main vortex. Higher Reynolds numbers placed the primary vortex in the upper right corner.

3.1.2. ***Case 2:*** *Opposite Direction Movement of Upper and Bottom Walls.*

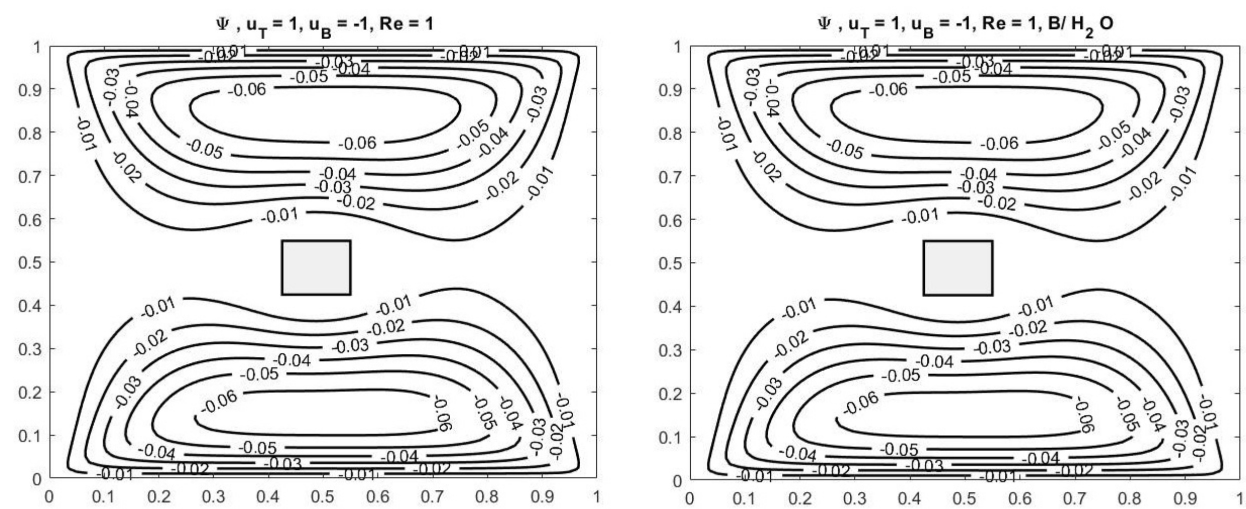

(I) (II)

Figure 8. The streamlines for Newtonian Fluid (I) and Boron/Water Nanofluid (II) at Re=1

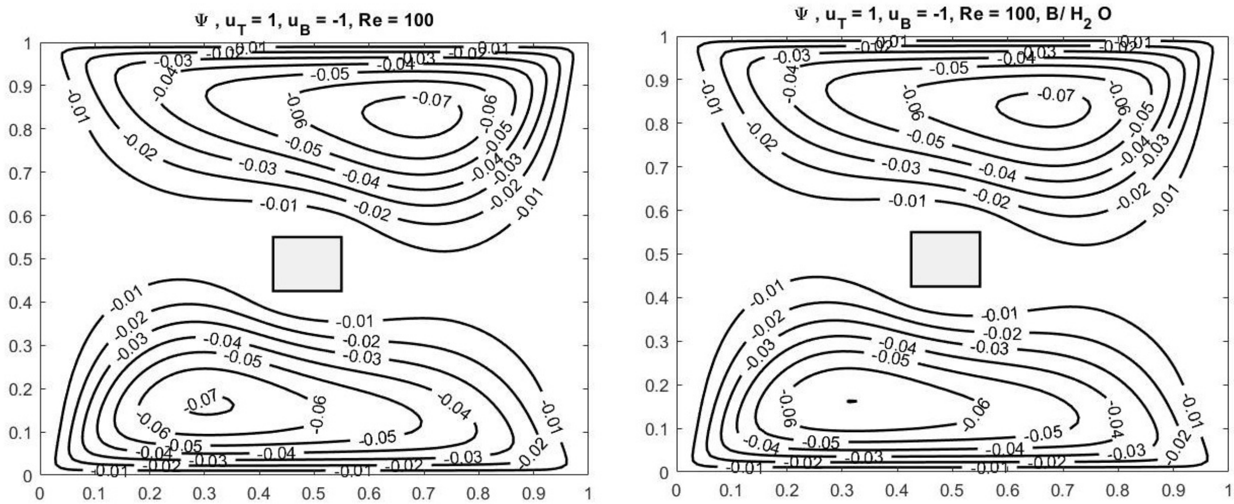

(i) (ii)

Figure 9. The streamlines for Newtonian Fluid (i) and Boron/Water Nanofluid (ii) at Re=100

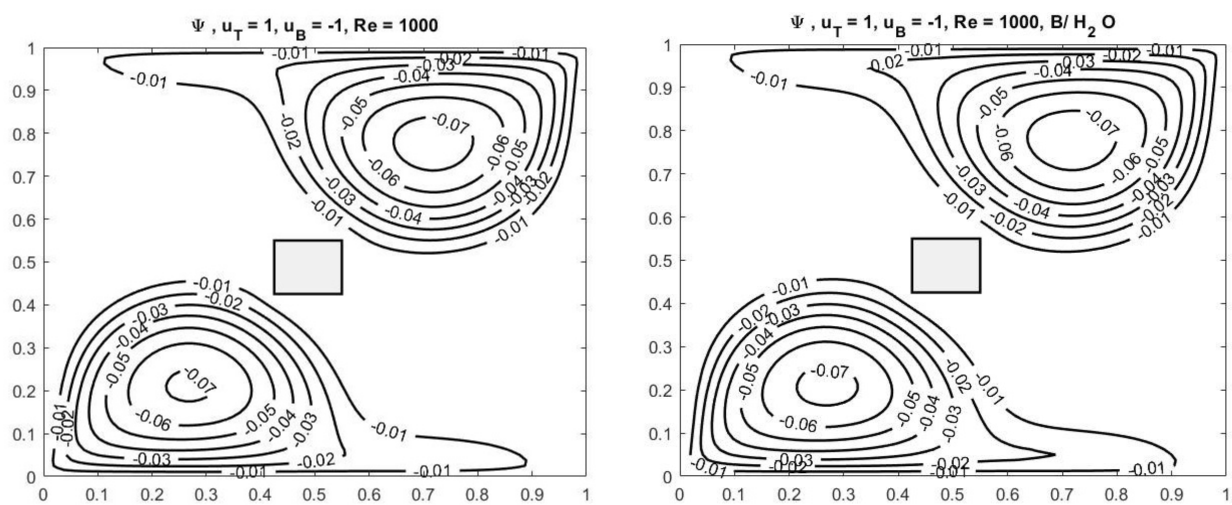

(i) (ii)

Figure 10. The streamlines for Newtonian Fluid (i) and Boron/Water Nanofluid (ii) at Re=1000

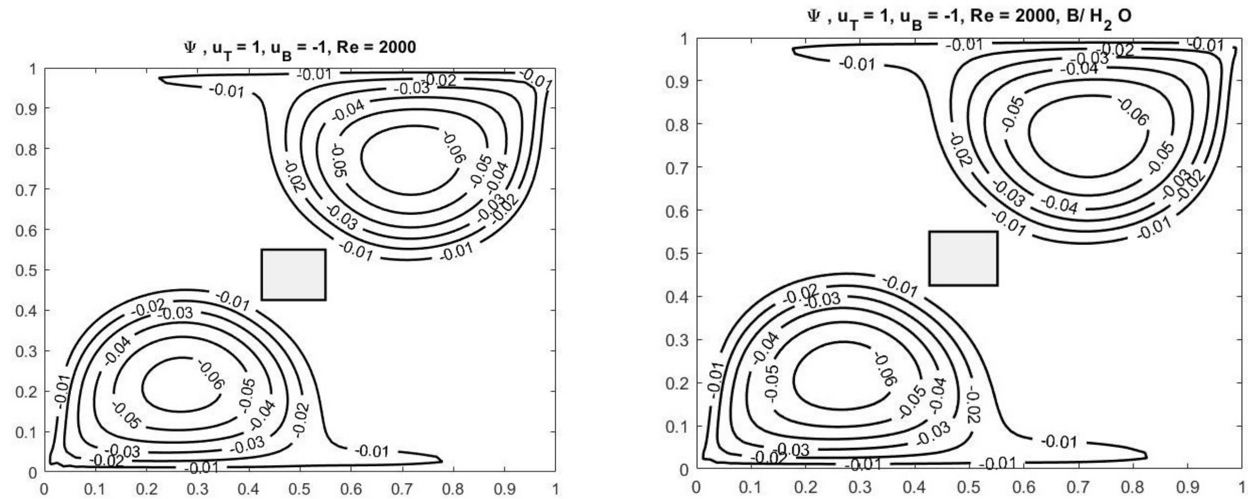

(I) (II)

Figure 11. The streamlines for Newtonian Fluid (I) and Boron/Water Nanofluid (II) at Re=2000

The graphical results of stream function contours for Newtonian fluid (I) and water-based Boron nanofluid (II) for Reynolds number values at 1,100,1000 and 2000 were given in Figures 8, 9, 10 and 11 respectively. The effect of walls moving in the opposite direction on the fluid was more clearly observed from the graphical results presented in Figures 9, 10 and 11. Additionally, as the Reynolds number increased, the impact of the obstacle on the streamlines became more pronounced.

3.1.3. ***Case 3:*** *Same Direction Movement of Upper and Bottom Walls.*

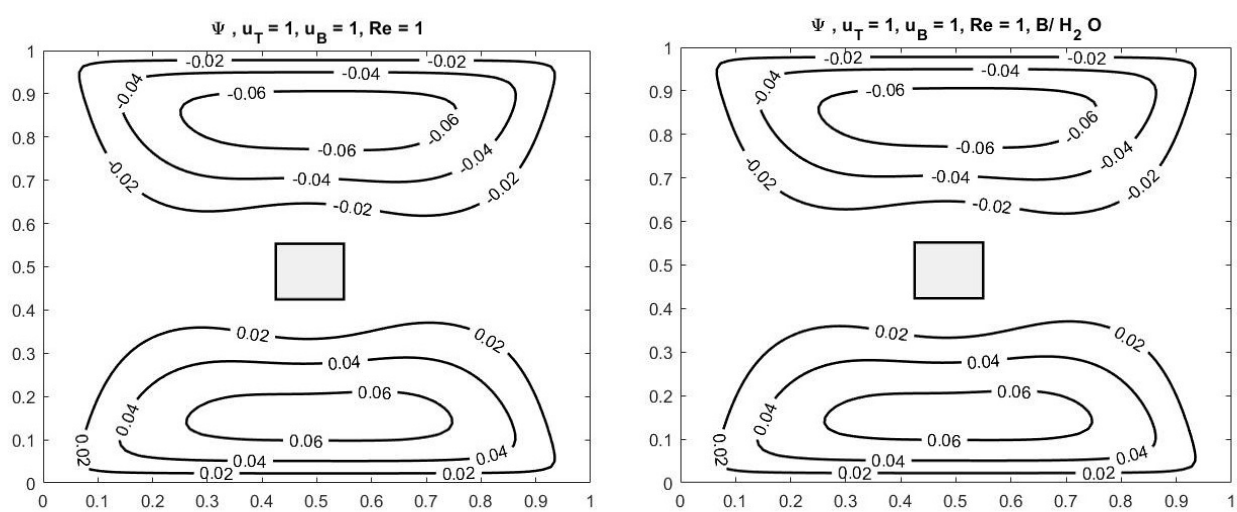

(I) (II)

Figure 12. The streamlines for Newtonian Fluid (I) and Boron/Water Nanofluid (II) at Re=1

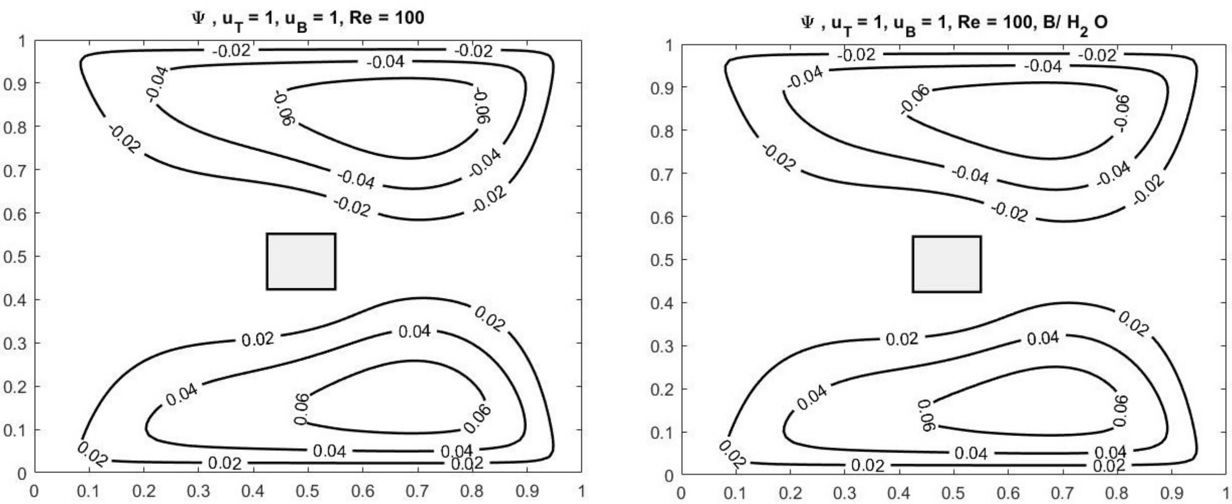

(i)

(ii)

FIGURE 13. The streamlines for Newtonian Fluid (i) and Boron/Water Nanofluid (ii) at Re=100

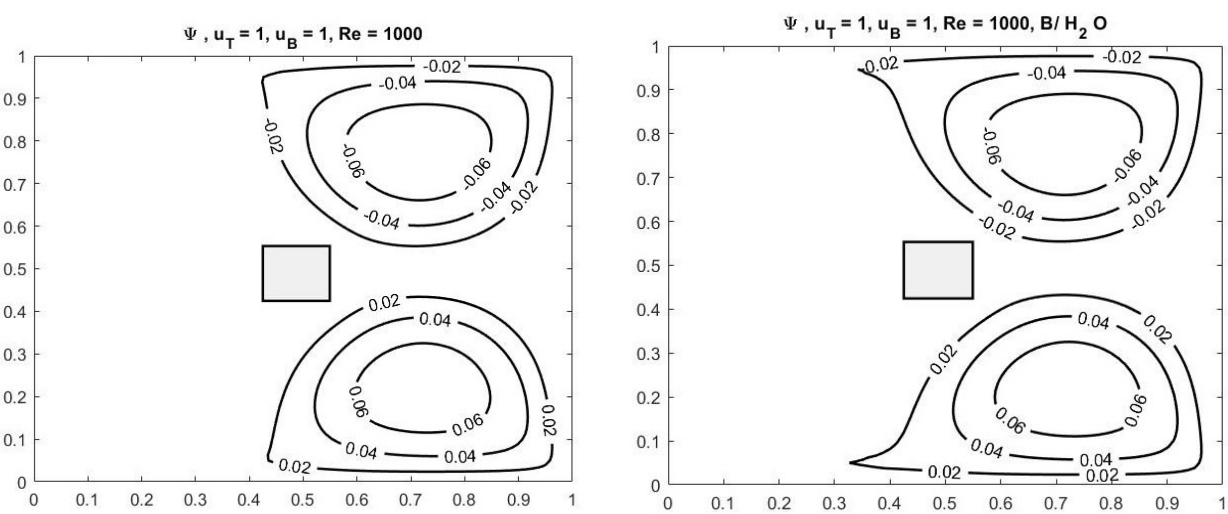

(i)

(ii)

FIGURE 14. The streamlines for Newtonian Fluid (i) and Boron/Water Nanofluid (ii) at Re=1000

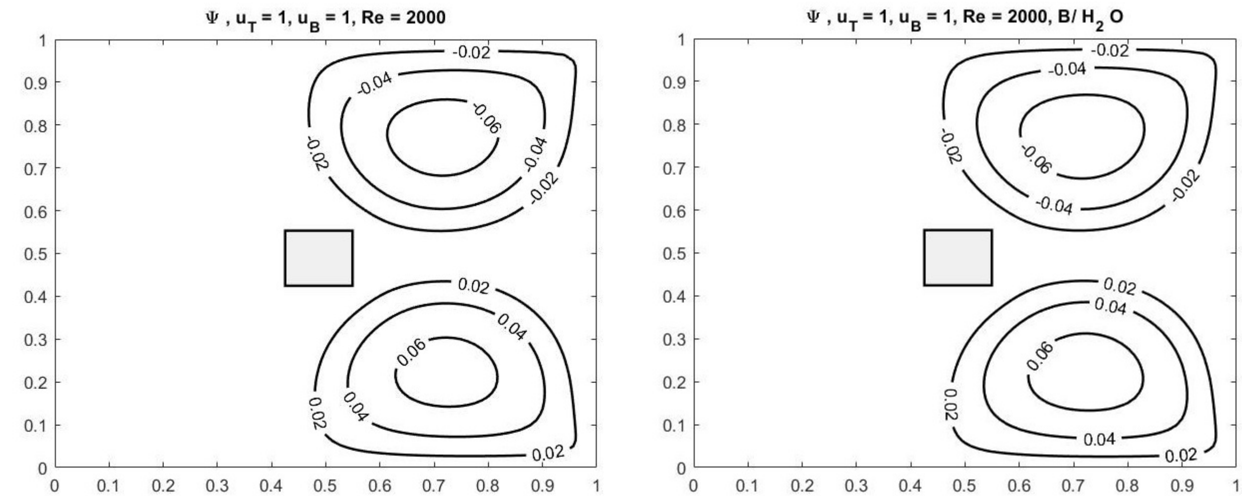

(i) (ii)

Figure 15. The streamlines for Newtonian Fluid (i) and Boron/Water Nanofluid (ii) at Re=2000

In Figures 12, 13, 14 and 15 the graphical representations of stream function contours for Newtonian fluid (i) and water-based Boron nanofluid (ii) were shown at the values of Reynolds number 1, 100, 1000 and 2000 respectively. The graphical differences were clearly observed in Figures 14 and 15. With increasing values of the Reynolds number, the streamlines became more concentrated on the right side of the cavity. Additionally, the vortex grew larger and some streamlines appeared more defined. The graphical changes in the behaviour of the streamlines due to the obstacle in the cavity were clearly observable in Figures 12 and 13. As the Reynolds number increased, the streamlines shifted further to the right side of the obstacle.

3.2. **Comparison of Streamlines When Aspect Ratio is 0.33.**

3.2.1. ***Case 1:*** *Movement of Upper Wall.*

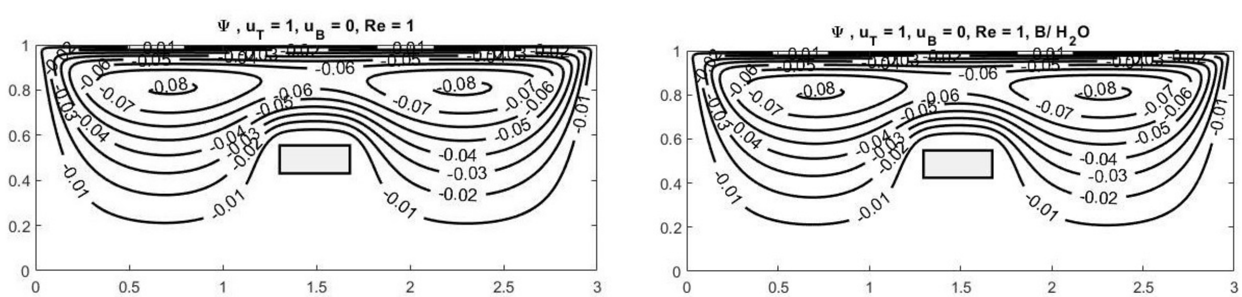

(i) (ii)

Figure 16. The streamlines for Newtonian Fluid (i) and Boron/Water Nanofluid (ii) at Re=1

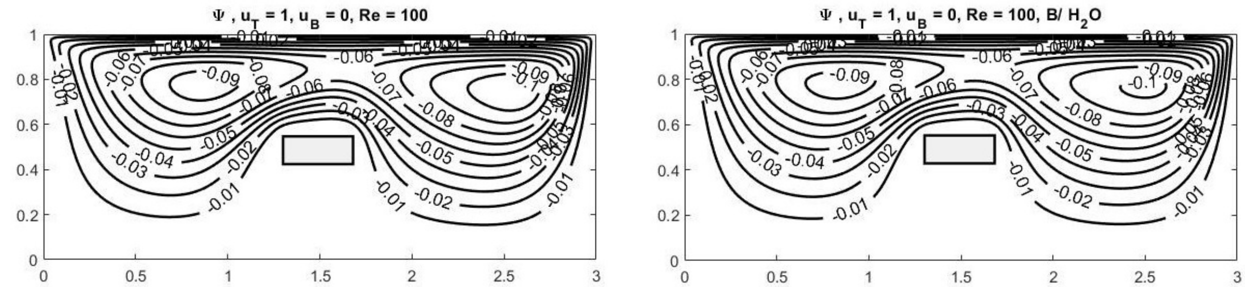

(I) (II)

FIGURE 17. The streamlines for Newtonian Fluid (I) and Boron/Water Nanofluid (II) at Re=100

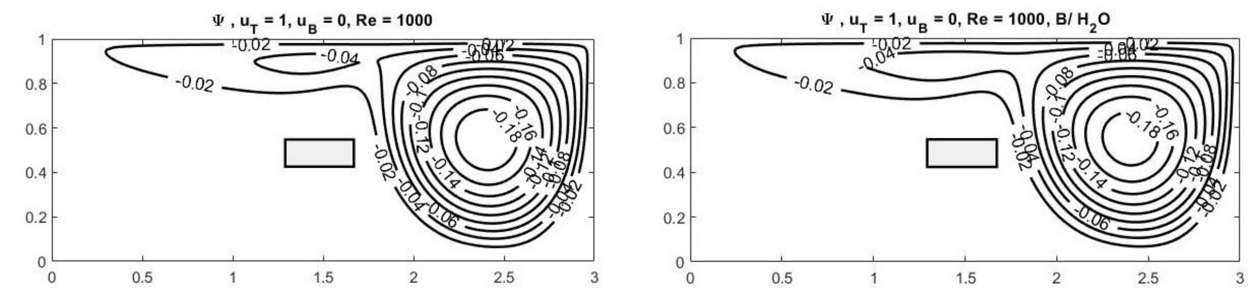

(I) (II)

FIGURE 18. The streamlines for Newtonian Fluid (I) and Boron/Water Nanofluid (II) at Re=1000

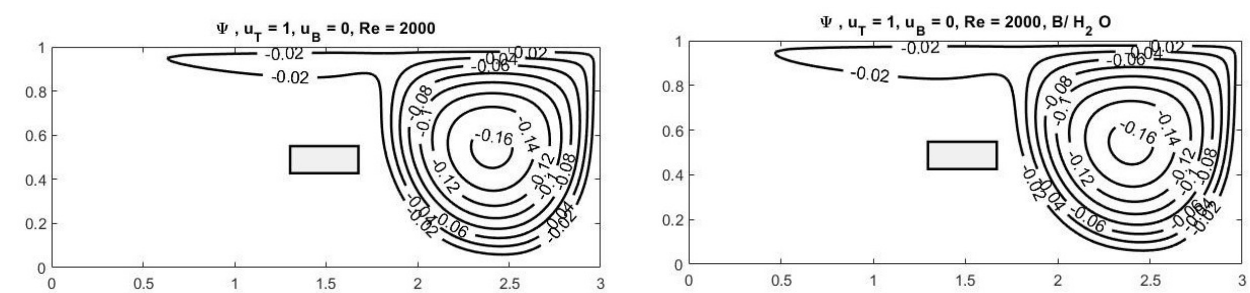

(I) (II)

FIGURE 19. The streamlines for Newtonian Fluid (I) and Boron/Water Nanofluid (II) at Re=2000

In Figures 16, 17, 18 and 19 the graphical representations of stream function contours when the aspect ratio was 0.33 were shown at the Reynolds number 1, 100, 1000 and 2000 values, respectively. The effect of the obstacle inside the region was clearly seen in Figures 16 and 17. Two different vortex centers were formed to the left and right of the obstacle. The resulting shape was that of a suppressed vortex that was split in two by the effect of the obstacle but merged at the top of the obstacle. In Figures 18 and 19, due to the effect of increasing the Reynolds number, the vortices merged to form a single vortex on the right side of the region. The vortex was located on the top and right side of the region independently of the obstacle.

3.2.2. ***Case 2:*** *Opposite Direction Movement of Upper and Bottom Walls.*

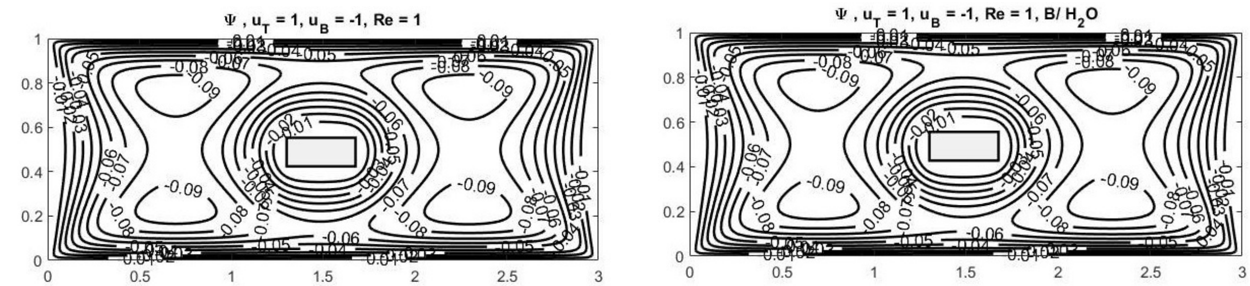

(i) (ii)

Figure 20. The streamlines for Newtonian Fluid (i) and Boron/Water Nanofluid (ii) at Re=1

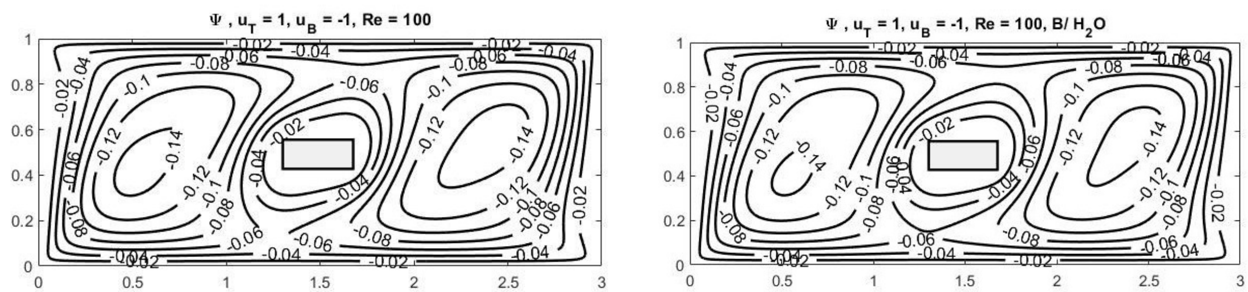

(i) (ii)

Figure 21. The streamlines for Newtonian Fluid (i) and Boron/Water Nanofluid (ii) at Re=100

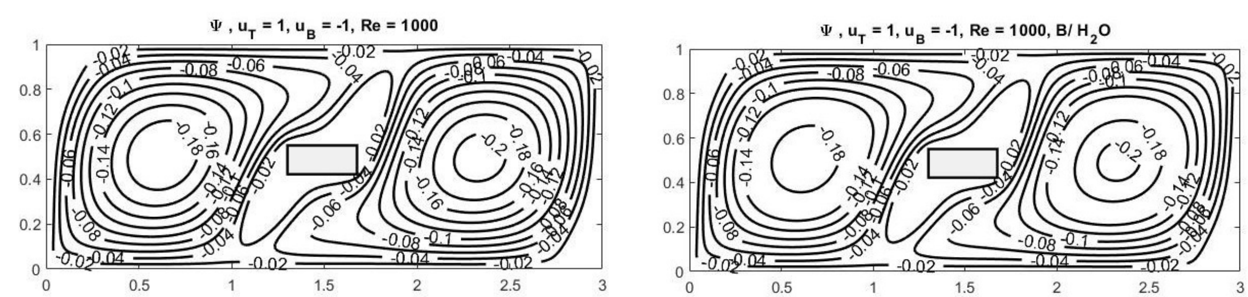

(i) (ii)

Figure 22. The streamlines for Newtonian Fluid (i) and Boron/Water Nanofluid (ii) at Re=1000

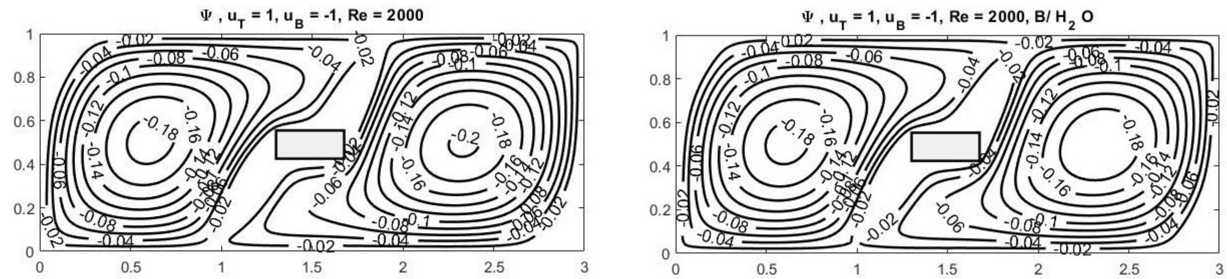

(i) (ii)

FIGURE 23. The streamlines for Newtonian Fluid (i) and Boron/Water Nanofluid (ii) at Re=2000

In Figures 20, 21, 22 and 23 the graphical representations of the contours of the stream function for Newtonian fluid (i) and water-based Boron nanofluid (ii) were shown in Reynolds number 1, 100, 1000 and 2000 respectively. In Figure 20 it was observed that a five-vortex-centered structure emerged. This remarkable result was described as a double hourglass formation. Furthermore, the formation of completely symmetrical vortices around the obstacle in Figure 20 was seen as a significantly different outcome. In Figures 21, 22 and 23, which presented the graphical results of this situation, it was observed that vortex structures with two centers of different sizes formed and symmetrical streamlines appeared around the obstacle.

3.2.3. ***Case 3:*** *Same Direction Movement of Upper and Bottom Walls.*

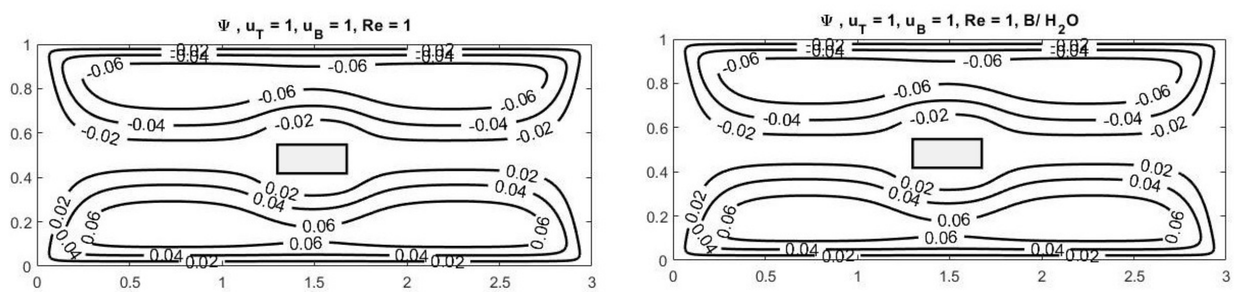

(i) (ii)

FIGURE 24. The streamlines for Newtonian Fluid (i) and Boron/Water Nanofluid (ii) at Re=1

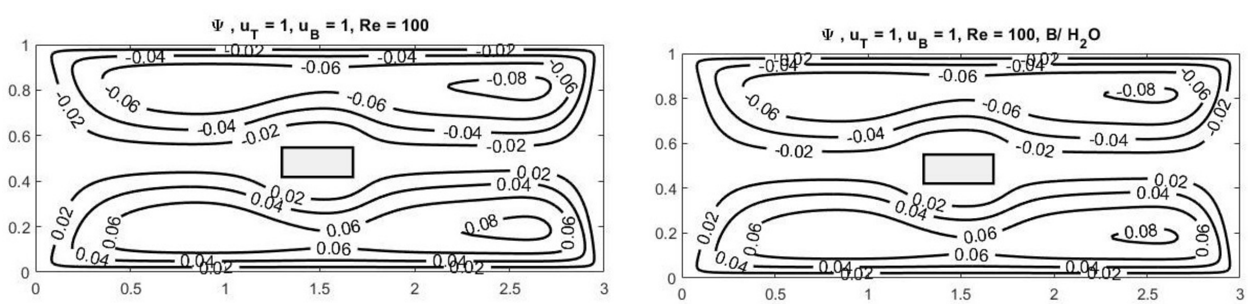

(i) (ii)

FIGURE 25. The streamlines for Newtonian Fluid (i) and Boron/Water Nanofluid (ii) at Re=100

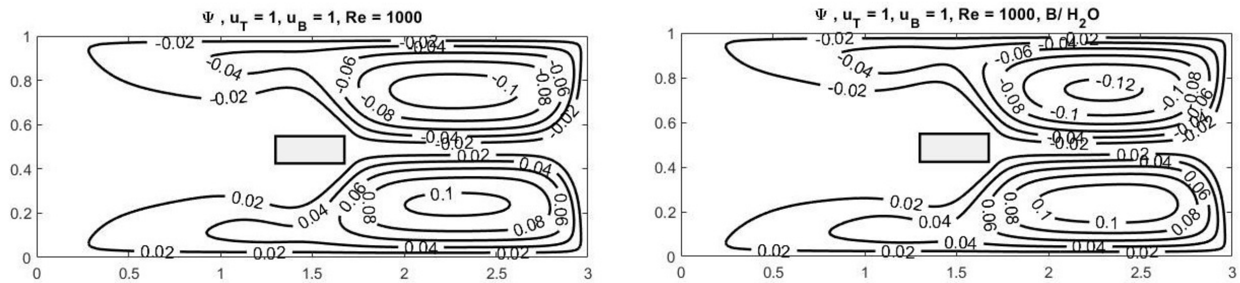

(i) (ii)

Figure 26. The streamlines for Newtonian Fluid (i) and Boron/Water Nanofluid (ii) at Re=1000

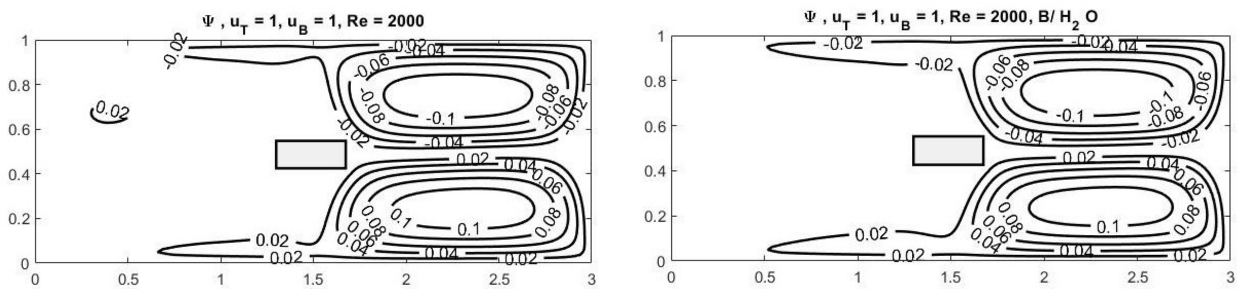

(i) (ii)

Figure 27. The streamlines for Newtonian Fluid (i) and Boron/Water Nanofluid (ii) at Re=2000

In Figures 24, 25, 26 and 27 the graphical representations of stream function contours for Newtonian fluid (i) and water-based Boron nanofluid (ii) were shown at the values of Reynolds number 1, 100, 1000 and 2000 respectively. The differences between the Newtonian fluid and the nanofluid were relatively small in Figures 24 and 25. However, the effect of the Reynolds number was clearly observed in Figures 26 and 27. This effect had not been as apparent in the previous streamlines at Reynolds numbers of 1000 and 2000 examined in this study. The changes observed at these values were attributed to the aspect ratio and the presence of the obstacle in the region.

4. Conclusion

In this study, numerical simulations were performed to illustrate the effects of moving walls on the flow dynamics within a cavity, with aspect ratios of 1 and 0.33, and influenced by a centrally positioned obstacle. The governing equations of motion were discretized using the finite difference method and solved with the Successive Over-Relaxation (SOR) method. To systematically analyse the influence of wall motion on the flow behaviour, three distinct cases were evaluated:

Case 1: The upper wall was in motion, while the bottom wall remained stationary. This case enabled a detailed investigation of the flow dynamics under these specific boundary conditions, serving as a baseline for comparison with other cases.

Case 2: The upper and bottom walls were actuated in opposite directions, resulting in a differential flow response. This configuration allowed for the exploration of more complex flow interactions and their influence on the overall flow structure within the cavity.

Case 3: Both the upper and bottom walls moved synchronously in the same direction, creating a uniform flow pattern. This configuration provided an opportunity for an in-depth analysis of the effects of synchronized wall motion on the flow characteristics, offering valuable insights into the fluid behaviour under coordinated boundary movements.

Each of these cases was carefully chosen to provide a comprehensive perspective of the influence of wall motion together with an obstacle inside the cavity on the flow dynamics. The velocity profiles for Newtonian fluid flow were obtained and found to be in line with the results reported in the literature. These results show that the nanofluid does not have much influence on the flow in the square cavity region regardless of any Reynolds number. In all three cases, the influence of the obstacle on the flow field was found to be considerable. This effect was clearly illustrated in Figure 20, where the fluid behaviour deviated from the classical expectations typically observed in similar systems. Furthermore, the modification of the aspect ratio to 0.33 was found to markedly affect the streamlines. As indicated by the results, the flow either concentrated around the obstacle or bypassed it. In Case 2, highly symmetric flow patterns were observed. As the Reynolds number increased, the flow was observed to shift toward the right side of the cavity, with the vortex also shifting in the same direction.

The SOR method was verified to be an effective tool for numerical solutions of nanofluid equations. The newly developed simulation code was shown to be highly efficient in combining the Finite Difference Method with the SOR technique, providing reliable, rapid, and consistent results, despite the instability effects caused by the obstacle. The performance of the algorithm was found to be highly dependent on both the aspect ratio and Reynolds number. Consequently, the results of present study highlight the significant impact of wall motion and obstacle-induced effects on fluid behaviour, particularly under varying Reynolds numbers. The findings of this work contribute valuable insights into the dynamics of nanofluids in confined geometries and advance the development of more efficient numerical modelling techniques for such systems. The current study also opens the possibility for the application of advanced optimization algorithms to optimize the design of cavities and flow systems based on nanofluid properties. In addition, the combination of the simulation code developed with the experimental data could serve to validate and refine the numerical models, improving their predictive accuracy. The findings presented here could also be extended to industrial applications such as heat exchangers, cooling systems and microfluidic devices, where the precise control of fluid flow and thermal behaviour is critical.

This study is derived from Yucel Balturk's PhD Thesis titled Numerical solutions of nanofluids in cavity flow with various aspect ratios dated March/2023 at Ondokuz Mayis University.

Conflicts of Interest

The authors declare that there are no conflicts of interest regarding the publication of this article.

Authors Contribution Statement

The authors have read and agreed to the published version of the manuscript.

References

[1] Abad, J.M.N., Alizadeh, R., Fattahi, A., Doranehgard, M.H., Alhajri, E. et al. *Analysis of transport processes in a reacting flow of hybrid nanofluid around a bluff-body embedded in porous media using artificial neural network and particle swarm optimization*, Journal of Molecular Liquids, **313**(2020), 113492.

[2] Batchelor, G.K., *On steady laminar flow with closed streamlines at large Reynolds number*, Journal of Fluid Mechanics, **1**(2)(1956), 177–190.

[3] Brinkman, H.C., *The viscosity of concentrated suspensions and solutions*, The Journal of chemical physics, **20**(4)(1952), 571–571.

[4] Burggraf, O.R., *Analytical and numerical studies of the structure of steady separated flows*, Journal of Fluid Mechanics, **24**(1)(1966), 113–151.

[5] Cacua, K., Buitrago-Sierra, R., Pabón, E., Gallego, A., Zapata, C. et al. *Nanofluids stability effect on a thermosyphon thermal performance*, International Journal of Thermal Sciences, **153**(2020), 106347.

[6] Chien, W.L., Rising, H., Ottino, J.M., *Laminar mixing and chaotic mixing in several cavity flows*, Journal of Fluid Mechanics, **170**(1986), 355–377.

[7] Çilingir Süngü, İ., Kapalı Bölgede Duvar Hareketli Akış ve Doğal Taşınımlı Isı Geçişinin Sayısal Çözümü, Ph. D. Thesis, Ondokuz Mayıs University, Institute of Science and Technology, Department of Mathematics, Samsun, Türkiye, 2011.

[8] Demir, H., The Stability Properties of Some Rheological Flows, Ph. D. Thesis, The University of Glamorgan, School of Accounting and Mathematics, Divison of Maths and Computing, 264, Wales (Galler), UK, 1996.

[9] Jana, S.C., Metcalfe, G., Ottino, J.M., *Experimental and computational studies of mixing in complex Stokes flows: the vortex mixing flow and multicellular cavity flows*, Journal of Fluid Mechanics, **269**(1994), 199–246.

[10] Kawaguti, M., *Numerical solution of the Navier-Stokes equations for the flow in a two-dimensional cavity*, Journal of the Physical Society of Japan, **16**(11)(1961), 2307–2315.

[11] Li, Q., Xuan, Y., Wang, J., *Experimental investigations on transport properties of magnetic fluids*, Experimental Thermal and Fluid Science, **30**(2)(2005), 109–116.

[12] Mahmoodi, M., Abbasian, A.A.A., Mazrouei, S.S., Nazari, S., Akbari, M., *Free convection of a nanoluid in a square cavity with a heat source on the bottom wall and partially cooled from sides*, Thermal Science, **18**(2)(2014), 283–300.

[13] Öztop, H.F., Al-Salem, K., Pop, I., *MHD mixed convection in a lid-driven cavity with corner heater*, International Journal of Heat and Mass Transfer, **54**(15-16)(2011), 3494–3504.
[14] Pan, F., Acrivos, A., *Steady flows in rectangular cavities*, Journal of Fluid Mechanics, **28**(4)(1967), 643–655.
[15] Peaceman, D.W., Rachford, Jr, H.H., *The numerical solution of parabolic and elliptic differential equations*, Journal of the Society for industrial and Applied Mathematics, **3**(1)(1955), 28–41.
[16] Şahin, B., *Bor nanoparçacıklarının doğal taşınımla ısı transferinde nanoakışkan olarak kullanımının incelenmesi ve karşılaştırılması*, Dokuz Eylül Üniversitesi Mühendislik Fakültesi Fen ve Mühendislik Dergisi, **22**(66)(2020), 701–714.
[17] Tosaka, N., Kakuda, K., *Development of BEM for convective viscous flow problems*, International Journal of Solids and Structures, **31**(12-13)(1994), 1847–1859.
[18] Tuann, S.Y., Olson M.D., *Review of computing methods for recirculating flows*, Journal of Computational Physics, **29**(1)(1978), 1–19.